

High Spatial Resolution X-Ray Spectroscopy of Cas A with *Chandra* *

Xue-Juan Yang^{1,2}, Fang-Jun Lu¹ and Li Chen²

¹ Particle Astrophysics Center, Institute of High Energy Physics, Chinese Academy of Sciences, Beijing 100049, China; yangxj@mail.ihep.ac.cn

² Department of Astronomy, Beijing Normal University, Beijing 100875, China

Received 2007 October 7; accepted 2007 November 20

Abstract We present high spatial resolution X-ray spectroscopy of the supernova remnant Cassiopeia A with the *Chandra* observations. The X-ray emitting region of this remnant was divided into 38×34 pixels of $10'' \times 10''$ each. Spectra of 960 pixels were created and fitted with an absorbed two component non-equilibrium ionization model. From the results of the spectral analysis we obtained maps of absorbing column density, temperatures, ionization ages, and the abundances of Ne, Mg, Si, S, Ca and Fe. The Si, S and possibly Ca abundance maps show obvious jet structures, while Fe does not follow the jet but seems to be distributed perpendicular to it. The abundances of Si, S and Ca show tight correlations between one another over a range of about two dex. This suggests that they are ejecta from explosive O-burning and incomplete Si-burning. Meanwhile, the Ne abundance is well correlated with that of Mg, indicating them to be the ashes of explosive C/Ne burning. The Fe abundance is positively correlated with that of Si when the latter is lower than 3 times the solar value, and is negatively correlated when higher. We suggest that such a two phase correlation is due to the different ways in which Fe was synthesized.

Key words: ISM: supernova remnants —ISM: individual: Cassiopeia A

1 INTRODUCTION

The young core-collapse supernova remnant (SNR) Cassiopeia A (Cas A) is regarded as a perfect laboratory for studying the ejecta and shock in SNRs, for its age and distance are well-determined and its radiations are very bright across the whole electromagnetic spectrum. The age of Cas A is around 300 years (Thorstensen et al. 2001) and the distance about 3.4 kpc (Reed et al. 1995). It appears today as a bright, nearly circular 3 arcmin diameter ring, with a low surface brightness 5 arcmin diameter radio and X-ray plateau. As a young SNR, it is believed that the thermal X-ray emission mainly comes from the forward shocked interstellar medium (ISM) (Shklovsky 1973) and the reverse shocked supernova (SN) ejecta (McKee 1974). The X-ray image of Cas A is consistent with this scenario as pointed out by Gotthelf et al. (2001): they discovered a thin, bright X-ray wisp that is interpreted as the forward shock, and a sharp rise in radio and X-ray line emissivity at the inner edge of the bright ring, which is associated with the reverse shock.

The numerical models (e.g., Woosley & Weaver 1995; Thielemann et al. 1996) predict that nucleosynthesis in core-collapse supernovae (SNe) occurs in an “onionskin” manner. Explosive Si burning occurs near the core, where the shock temperatures is the highest. This process would burn up Si and form ejecta dominated by ^{56}Ni , which decays to ^{56}Co and finally ^{56}Fe . Further, as the shock temperature decreases, Si burning becomes incomplete and the main products include not only Fe, but also much Si, S, Ar and Ca. Even further out, explosive O burning occurs, leading to a composition dominated by O and Si with very

* Supported by the National Natural Science Foundation of China.

little or no Fe. At the outmost layer, explosive Ne/C burning occurs and forms mostly O. Willingale et al. (2002) did a spectral mapping of Cas A using the data collected by the XMM-Newton X-ray observatory (*XMM-Newton*). They found that the distributions of Si, S, Ar and Ca are very similar to each other but distinct from Ne and Mg. This supports the above explosive nucleosynthesis network. However, Hughes et al. (2000) and Willingale et al. (2002), using data from the Chandra X-ray observatory (*Chandra*) and *XMM-Newton* respectively, showed that the Fe-rich ejecta lie outside the Si-rich material. It was concluded that the ejecta in Cas A have undergone a spatial inversion of the explosive O- and Si-burning products. That is to say, the materials from the predicted “onion” layers have become mixed together. Hughes et al. (2000) proposed this inversion to be the result of neutrino-driven convection during the initiation of the SN explosion.

Chandra carried out a 1 Ms observation on Cas A as a Very Large Project (VLP), which was largely motivated by the two papers: Laming & Hwang (2003) and Hwang & Laming (2003), focusing on the suggested jet structure of the ejecta and the iron synthesis. Hwang et al. (2004) showed the first results of these observations. A jet structure of the Si-rich ejecta was clearly found in the enhanced Si-K emission line image. So it was proposed that Cas A was formed by an asymmetric explosion, which is also indicated by the observed kinematics and the high ^{44}Ti yield (Vink 2004). Fe-rich ejecta, however, were not found in the jet area, but perpendicular to it instead. This contradicts the jet-induced explosion (Khokhlov et al. 1999), but might be the case for collapsars (Nagataki et al. 2003; Zhang et al. 2004). The explosion energy for Cas A was about $2 \sim 4 \times 10^{51}$ erg, suggesting it to be a normal SN (Laming & Hwang 2003). Cas A thus provides strong evidence that jets may also be produced by normal SNe (Hwang et al. 2004).

In this paper, we present high resolution X-ray spectroscopy of Cas A using the *Chandra* observations. Willingale et al. (2002) did a similar work with the *XMM-Newton* data. Here we would like to cross-check their results. In our work, we use a smaller pixel size ($10'' \times 10''$, 1/4 of that used by Willingale et al. 2002), which is closer to the typical size of the ejecta knots of Cas A. Another point is that the so-called “jet” region is included in the analysis, which was not included in Willingale et al. (2002). The high spatial and spectral resolutions of *Chandra* together with the abundant archived data permit us to study this famous SNR in detail. In Section 2, we describe the observation and data reduction. In Section 3 we show the results, while some discussion is presented in Section 4, and a summary in Section 5.

2 OBSERVATION AND DATA REDUCTION

Cas A was observed by *Chandra* for about 1 Ms in 2004 as a VLP. The details of the observations were described by Hwang et al. (2004). In this paper, we use data from two deep ACIS exposure segments of the VLP. One was performed from April 14 to 16 (Observation ID: 4638) and the other from May 25 to 26 (Observation ID: 4639), with exposure times of about 167 ks and 80 ks, respectively. The reasons that we used two segments are to ensure good statistics for the spatially resolved analysis and to reduce the mis-calibration effects, by using data collected at different epochs.

The X-ray data were analyzed using the software package CIAO (version 3.3, with the CALDB version 3.2.1 and the ATOMDB version 1.3.1). For our analysis, the X-ray emission region was divided into “pixels” with size about $10'' \times 10''$, corresponding to a 38×34 grid. Figure 1 shows the image for observation ID 4639 with the grid overlaid. We retained events within energy range 0.5–10 keV using the archived level 2 event file and created spectra for 960 pixels that contain at least 3000 counts. The frequency distribution of the counts in each pixel is shown in Figure 2 (left panel). We can see that most pixels contain more than 10000 counts, which allows high statistical analysis. The background spectrum was created from the off-source region.

The spectral analysis was performed using the XSPEC (version 11.2) package (Arnaud 1996). The spectra for each pixel of the two observations were jointly fitted with two non-equilibrium ionization components (VNEI, Borkowski et al. 2001). The free parameters are the temperatures, emission measures, ionization ages ($\tau = n_e t$) and abundances of O, Ne, Mg, Si, S, Ca and Fe for each of the two components. The abundances are in units of the solar abundances given by Anders & Grevesse (1989). We also introduced a uniform redshift for each component to study the dynamics. The WABS model (Morrison & MacCammon 1983) was included to take care of interstellar photo-electric absorption. A Gaussian line was added at the energy of 3.4 keV to allow for the Ar line emission, which is not included in the VNEI model in XSPEC version 11.2 we used.

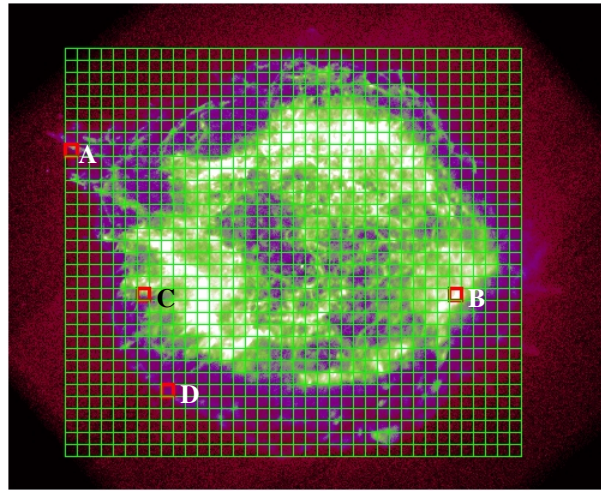


Fig. 1 Pixel grid used in our analyses is superimposed on the *Chandra* image of Cas A (Observation ID: 4639). Region A, B, C and D are described in Sect. 3 and their spectra are presented in Fig. 3.

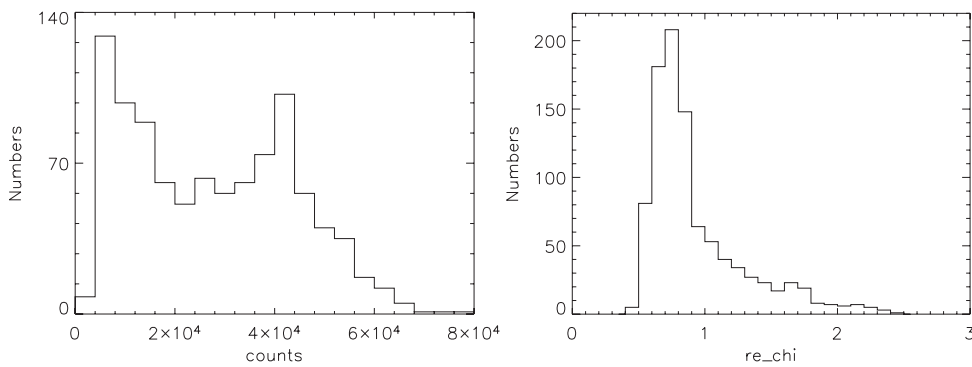


Fig. 2 Frequency distributions of the 960 pixel counts (left panel) and χ^2 values obtained in the spectra fits (right panel).

Here we note two points. One is that the nonthermal emission undoubtedly contributes to the 4 ~ 6 keV continuum, which could be as high as 25% in Cas A (Willingale et al. 2002). However, since its X-ray emission is dominated by the thermal component (Laming 2001; Bleeker et al. 2001) and we are mainly interested in the study of line emission in this paper, we believe that our model is appropriate. The same spectral model was also used by Willingale et al. (2002). The other point is that Cas A is an O-rich SNR, so that O contributes a significant fraction of the electrons (Vink et al. 1996; Willingale et al. 2002). In this case, the O abundance is coupled with the emission measure. Here we set the O abundances of both components as free parameters in the fitting process, but we will not discuss the O abundance in this paper as it might be contaminated.

3 RESULTS

The frequency distribution of the 960 reduced χ^2 values of the spectral fits is given in Figure 2 (right panel). It has a peak around 0.7, which suggests our fitting results to be acceptable statistically. In Figure 3, we give the spectra along with the fitting residuals of several typical regions (marked in Fig. 1). The emission lines are also marked. Region A is located in the outermost, northeastern part of the jet. It has very strong Si,S,

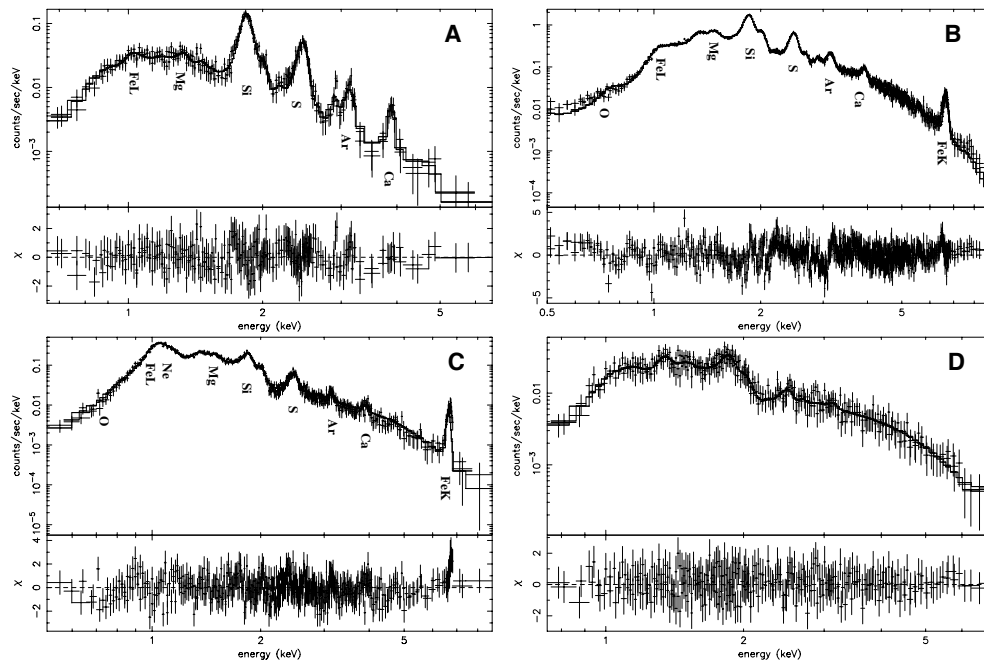


Fig. 3 Spectra from the regions marked in Fig. 1. Spectrum A represents the spectrum of the explosive O-burning products, while B and C, those of incomplete and complete explosive Si-burning products, respectively. Spectrum D is that of the forward shocked ISM.

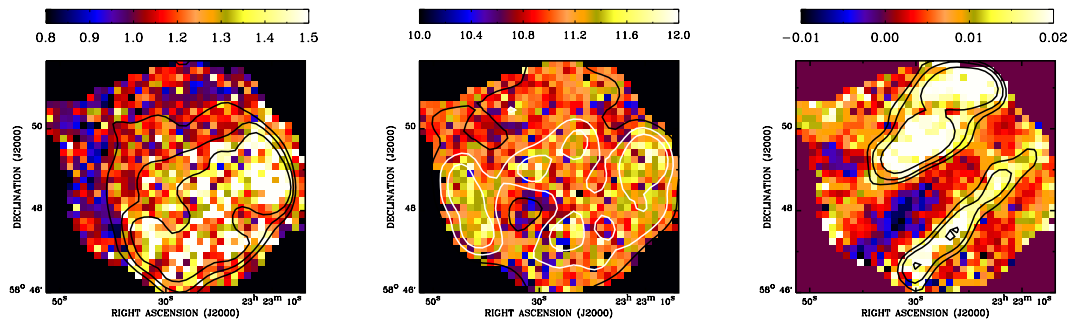


Fig. 4 Absorbing column density (N_{H} , 10^{22} cm^{-2} , left panel), ionization age ($\text{Log}_{10} n_e t \text{ cm}^{-3} \text{ s}$, middle panel), and red shift (right panel) maps of Cas A. The negative value of redshift means blueshift. The coding we used is shown on the top of each panel. The superimposed contours represent the same dataset, but after having been smoothed with a two-dimensional Gaussian with FWHM of $40'' \times 40''$. The contour levels are 1.1, 1.2, 1.3 for N_{H} ; 11.0, 11.2, 11.3 for $\text{Log}_{10} n_e t$; and 0.01, 0.012, 0.015 for redshift.

Ar and Ca lines, but the Fe-K line is absent. Therefore, it should be dominated by O-burning products, but we cannot rule out incomplete Si-burning, as there seem to be Fe-L lines around 1 keV (c.f. Sect. 1). Region B is from the counter-jet, which is very strong in Si and S. The Fe-K line is also obvious. This is entirely consistent with the incomplete Si-burning yield. Region C is the Fe-rich region in the southeast. From the spectra we can see very strong Fe-K and Fe-L lines, which are believed to be from complete explosive Si-burning. Region D is located at the outer rim, and it is weak in all the emission lines of the main elements in Cas A and is dominated by the continuum (cf. Hughes et al. 2000, fig. 3). These spectra show that the

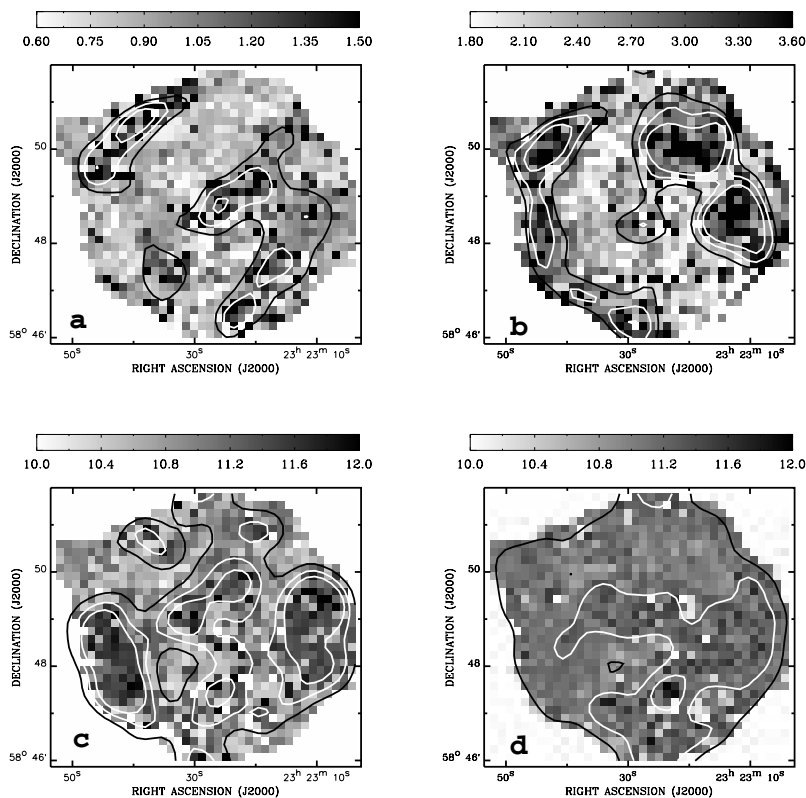


Fig. 5 Maps of temperatures and ionization ages for the cool (index 1) and hot (index 2) components of Cas A. a: kT_1 (keV), b: kT_2 (keV), c: $\text{Log}_{10}(n_e t)_1$ ($\text{cm}^{-3} \text{s}$), d: $\text{Log}_{10}(n_e t)_2$ ($\text{cm}^{-3} \text{s}$). The contours represent the corresponding images smoothed by the same Gaussian profile as in Fig. 4. Contour levels are 1.0, 1.1, 1.2 for kT_1 , 2.6, 2.8, 3.0 for kT_2 , and 11.0, 11.2, 11.3 for the two $\text{Log}_{10}(n_e t)$.

X-ray properties change significantly across the remnant. In the following we present the statistics of the spectral fitting results.

(1) We obtained the spatial distribution of the absorbing column density (Fig. 4), as well as the temperatures and ionization ages of the cool and hot components (Fig. 5). In order to show the large scale structures more clearly, we have smoothed all these maps with a two-dimensional Gaussian with FWHM $40'' \times 40''$, and superimposed the smoothed contours on the maps. The column density is higher in the western than the eastern part. This is consistent with the previous studies (Keohane et al. 1996; Willingale et al. 2002), in which it was suggested that the higher absorption to the west is due to the interaction of the remnant with the molecular cloud. The column density lies in the range $0.8 - 1.5 \times 10^{22} \text{cm}^{-2}$ with a mean value of $1.19 \times 10^{22} \text{cm}^{-2}$. The typical statistical error is $\sim 5\%$ at 90% confidence level. The column density is a little below the $1.50 \times 10^{22} \text{cm}^{-2}$ derived by Willingale et al. (2002), but is consistent with that from Keohane et al. (1996) given by the equivalent width of HI and OH ($1.05 - 1.26 \times 10^{22} \text{cm}^{-2}$).

The temperature distributions for the cool and hot components are somewhat dissimilar. It seems that the higher temperature of the hot components appears at the outer rim and in the Fe-rich regions (Fig. 6). This is not surprising, since the hot component is responsible for most of the Fe K emission and also dominates continuum above 4 keV (Willingale et al. 2002).

The ionization age maps for both components are very similar to the corresponding ones given by Willingale et al. (2002). We can see that the map of the hot component is relatively uniform over the whole remnant, while the cool one shows some structures. The brightest shell, which has the largest density, does

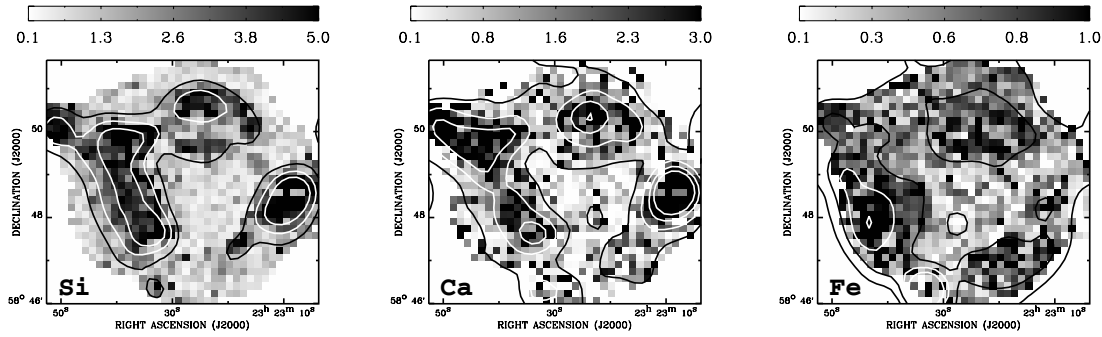


Fig. 6 Si, Ca and Fe abundance (in units of solar abundance) maps of Cas A. Superposed contours represent the same dataset but after having been smoothed with the same Gaussian profile as in Fig. 4. The contour levels are 2.0, 3.0, 4.0; 1.0, 2.0, 3.0, 4.0; and 0.3, 0.6, 0.9, 1.2, respectively.

Table 1 Coherent Coefficient for Data Points excluding Extremum Ones

Element	O	Ne	Mg	Si	S	Ca	Fe
O	–	0.33	0.41	0.33	0.26	0.14	0.13
Ne	0.33	–	0.49	0.19	0.16	0.05	0.25
Mg	0.41	0.49	–	0.48	0.39	0.16	0.24
Si	0.33	0.19	0.48	–	0.86	0.35	0.23
S	0.26	0.16	0.39	0.86	–	0.33	0.11
Ca	0.14	0.05	0.16	0.35	0.33	–	0.05
Fe	0.13	0.25	0.24	0.23	0.11	0.05	–

not have the highest ionization age. This leads to the conclusion that the brightest shell is shocked later. Considering that the cool component is associated with the reverse shock (Vink et al. 1996; Willingale et al. 2002), the reverse shocked ejecta may be stratified and so shocked at different times.

(2) We derived the spatial distributions of all the elements involved. The listed elemental abundance of each pixel is the mean of the two components weighted by their emission measures.

Figure 6 displays the abundance maps of Si, Ca and Fe. The contours have a similar meaning as those in Figure 4. We see that the Si, and possibly, the Ca abundances show a jet-like structure in the northeast and a counterpart in the southwest. This “jet” structure was first suggested in the Si emission line equivalent width image (Hwang et al. 2000) and was confirmed with the ratio images of Si, He, α (plus continuum, 1.78 ~ 2.0 keV) and 1.3 ~ 1.6 keV (mostly weak Mg, He α , Fe, L, plus continuum) (Hwang et al. 2004). Our abundance maps further confirm the results. Meanwhile, from the Fe abundance map, we can find that Fe is relatively poor in the jet area but seems to be rich in the direction perpendicular to it. It is also clearly shown in the map that Fe-rich knots lie outside the Si- and S-rich ejecta, which is consistent with the results of Hughes et al. (2000) and Willingale et al. (2002).

(3) Figures 7 – 9 are the correlation plots of the abundances of Ne, Si and Fe with the other elements. S is strongly correlated with Si. Its correlation with the other elements is very similar so is not displayed. We note that the minimum points are excluded, for they represent regions where emission from the continuum predominates, and the lines either do not show up or are very weak. In order to show more clearly the overall trends of the correlations, we binned the data points into 10 channels. The binned results are plotted with large pentacles in the figures. The corresponding correlation coefficients are given in Table 1. Apparently Si is well correlated with S, as well as with Ca. There is also a good correlation between Ne and Mg.

We noticed that in the abundance correlation diagram between Si and Fe, there seems to be a break at Si abundance 3: the correlation with Fe is positive or negative according as the Si abundance is less or greater

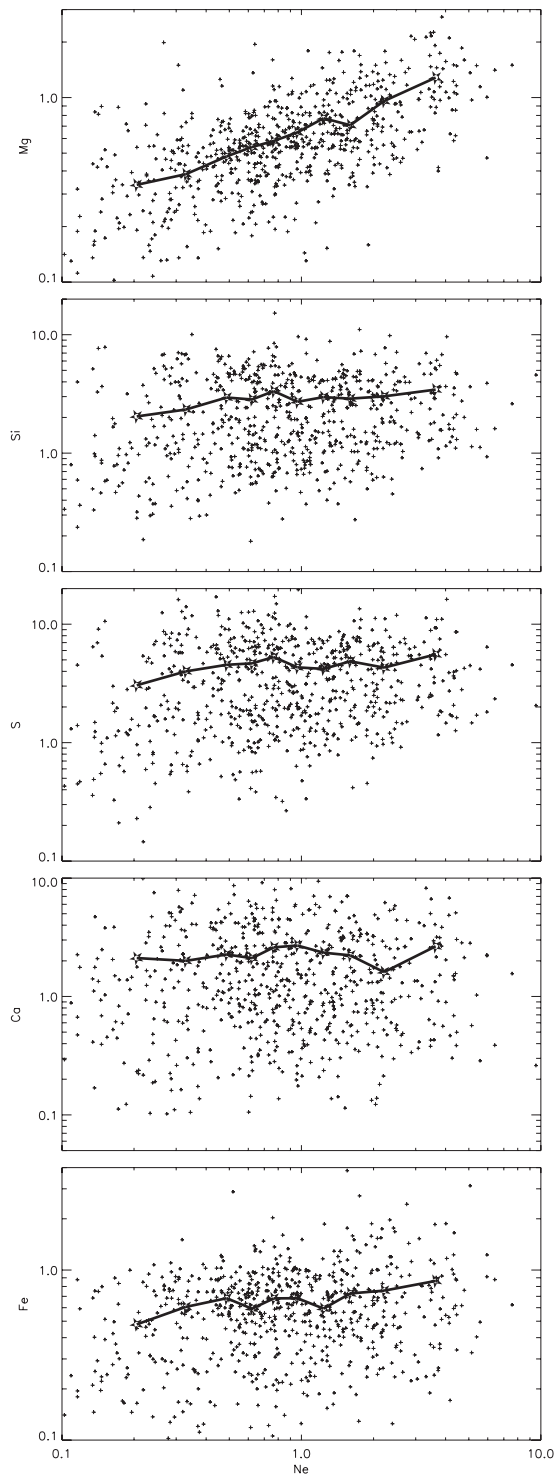


Fig. 7 Abundance correlation between Ne and the other elements. All the data points were binned into 10 channels and the binned results are plotted as large pentacles connected by the solid line.

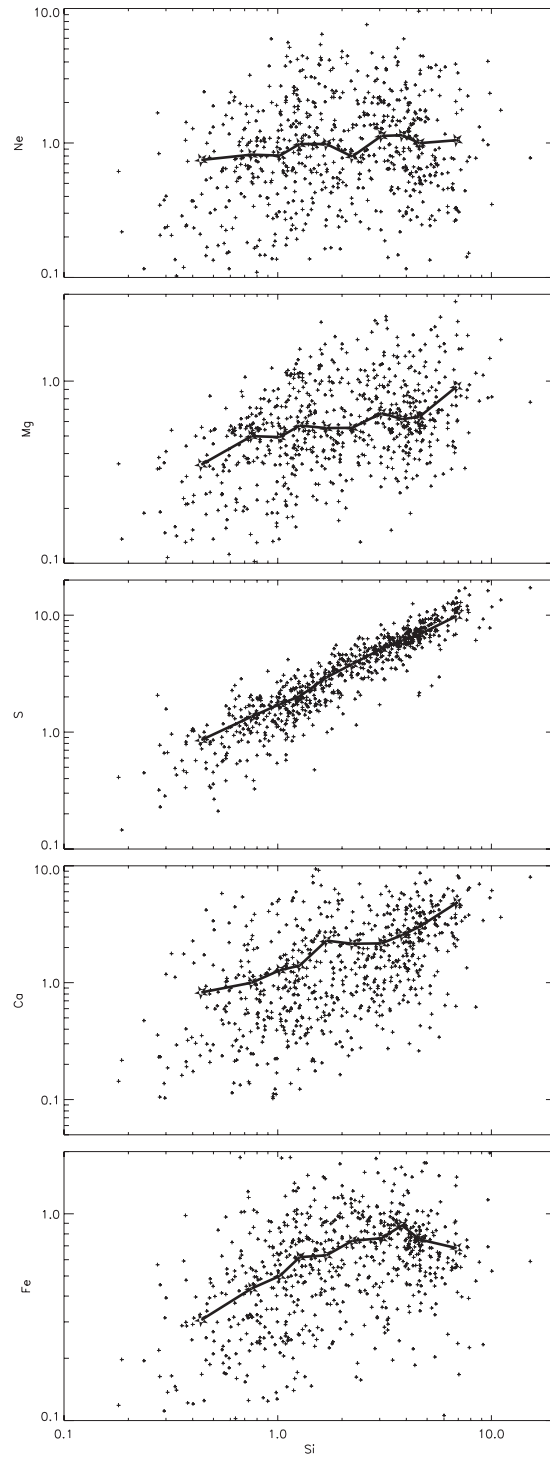


Fig. 8 Abundance correlation between Si and the other elements. The large pentacles and solid line have the same meaning as in Fig. 7.

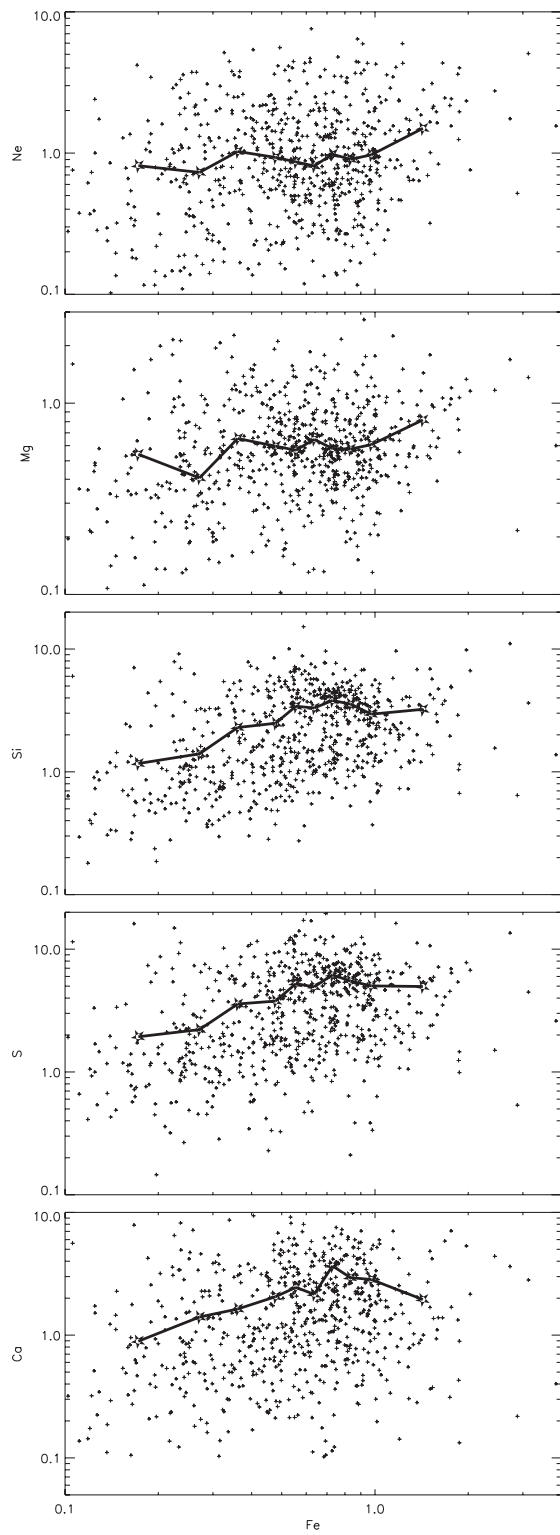


Fig. 9 Abundance correlation between Fe and the other elements. The large pentacles and solid line have the same meaning as in Fig. 7.

than 3. All these features should give us information on the (explosive) nucleosynthesis of the SN, as will be checked in detail in Section 4.3.

(4) The Doppler map (Fig. 4) we obtained is different from those of Willingale et al. (2002), who showed that the ejecta is generally blue shifted in the southeast, and redshifted in the north. However, in our map, only a small fraction in the southeast are blue shifted while most regions are red shifted. The Doppler map shows prominent “bar”-like features running from the southeast to the northeast.

We found that the Doppler map is mostly the result of mis-calibration. The direction of the “bar”-like feature is exactly along the CCD columns. Since the CCD pixels in one column share one read-out circuit, the red shift “bar” is probably due to the inefficiency of the read-out circuit. The generally accepted velocity for the knots is of the order of 2000 km s^{-1} (Willingale et al. 2002), corresponding to an energy shift of $\sim 15 \text{ eV}$ at 2 keV (near the Si and S lines). However, the resolution of *Chandra*-ACIS is about 150 eV , for which the calibration and/or the performance is probably not good enough to determine such a small energy shift. Therefore, we conclude that it is very difficult to derive a reliable Doppler map with the *Chandra*-ACIS data.

4 DISCUSSION

4.1 Jet Structure

The ejecta structure and the explosion asymmetry of Cas A have been widely studied. It has long been suggested that the core-collapse SN explosion process is intrinsically asymmetric, from both the observational and theoretical points of view (Khokhlov et al. 1999 and reference therein). For Cas A, it shows rapidly moving oxygen-rich material outside the nominal boundary (Fesen & Gunderson 1996) and evidence for two oppositely directed jets (Reed et al. 1999). The aspherical distribution of its ejecta suggests that the SN explosion which produced Cas A may be asymmetric.

Hwang et al. (2000, 2004) have further studied the jet emission of Si-rich ejecta using the *Chandra* data. These works are based on the equivalent width (EW) images of the emission lines. However, the correlation between the EW and the abundance can be distorted by temperature, column density and ionization age. In other words, the same abundance can be detected as significantly different EW because of the different line emissivity, which is a function of the local plasma conditions. Willingale et al. (2002) gave the abundance maps from the *XMM-Newton* data, and the jet structure is not seen in their results, due to the limited spatial resolution and bigger pixel size.

In this paper, we gave directly the element abundances map, among which Si, S and probably Ca show the jet structure as expected. The ejecta in the jet area are greatly enriched in Si, S and Ca, while relatively poor in Fe (still exists, c.f. Fig. 3B). This confirms not only the presence of jet itself but also that these elements come from incomplete explosive Si-burning rather than from O-burning (Khokhlov et al. 1999; Hughes et al. 2000). Meanwhile, Fe is less enriched in the counter-jet region (Fig. 3B) than in the off-jet area (Fig. 3C), which also implies that the jet material did not emerge from as deep in the progenitor as the other observed ejecta (Hughes et al. 2000 and reference therein).

4.2 Iron Distribution

As far as we know, ^{56}Fe mainly comes from the decay of ^{56}Ni , which is synthesized in the incomplete explosive Si-burning. Hwang & Laming (2003) identified a region of nearly pure Fe ejecta, which might be a candidate for the site of α -rich freezeout (see also Vink 2004). Early *Chandra* observations showed that the Fe emission in Cas A is associated with ejecta and is mainly distributed in the faint region outside the bright Si-dominated shell in the east. That the lack of Si beyond the Fe emission, as well as the lack of Fe inside the Si emission, argues against projection effects (Hughes et al. 2000).

From our abundance maps, we further confirmed that the ejecta highly enriched of Fe lie outside the Si and S dominated ejecta in the east. According to the onion model, the lighter an element is, the larger radius it should be located (Aschenbach 2002).

Since the projection effect may not play an important role, the fact that the Fe-rich materials lie outside the Si-rich ones means that the ejecta in Cas A may have suffered some kind of overturn, either during or after the explosion, which might be the result of the neutrino-driven convection during the initiation of the SN explosion (Hughes et al. 2000).

In the previous *Chandra* results (Hwang & Laming 2003; Laming & Hwang 2003), it has been suggested that the Fe-rich ejecta have a higher characteristic ionization age than the O/Si knots by factors of a few units up to 10, implying either a correspondingly higher density or an earlier shock time. As large density enhancement (or depletion) is subject to a number of hydrodynamic instabilities that might destroy the knots within a few shock crossing time scales (Klein et al. 1994; Klein et al. 2003; Wang & Chevalier 2001; Poludnenko et al. 2002; Poludnenko et al. 2004), such knots are thus not expected to be seen. So, Hwang & Laming (2003) claimed that early shock time and very modest (or no) density enhancement are the most consistent explanation for the Fe knots that survived to be seen today. Comparing Figure 4 (middle panel) and the Fe abundance map in Figure 6, we can find that the Fe-rich knots in the southeast do have a higher ionization age. This further confirms that they might be early shocked, and might provide additional evidence for the above mentioned overturn.

4.3 Nucleosynthesis

The abundances of Si, S and Ca show tight correlations with each other (Fig. 8) over a range of about two dex. Willingale et al. (2002) also presented similar results using the *XMM-Newton* data and the authors suggested the results to be strong evidence for the nucleosynthesis of these elements by explosive O-burning, and incomplete explosive Si-burning due to the shock heating of these layers in the core-collapse SN. The same degree of correlation can also be found between the abundances of Ne and Mg, which means that they might be the ashes of the explosive C/Ne burning. All these results are generally consistent with the (explosive) nucleosynthesis theory of a massive star (Woosley et al. 2002; Woosley & Janka 2006).

The Fe abundance is not correlated with any other element, with one exception that there seems to be a possible two phase correlation with Si (Figs. 8 and 9). It is contaminated by the extremum data points, for it is difficult to reliably derive the Fe abundances from the Fe L lines (e.g. Suh et al. 2005). So we picked regions whose spectra show clearly Fe K lines, and re-draw the Si versus Fe abundance plot in Figure 10. Now the two phase correlation is more clearly shown. From Figure 6 we can find that the regions with Si abundance higher than 3 are generally concentrated in the Si-dominated bright shell, which is natural, and also in the jet and its counterpart. These regions are believed to be the ejecta of incomplete explosive Si-burning or explosive O-burning. We know that explosive O-burning would lead to products with little or no Fe, while in the incomplete explosive Si-burning Fe is one of the main products. From the Si versus Fe correlation plot, we can see that Fe is not as enriched as Si, but still abundant. This would support these ejecta mainly coming from incomplete explosive Si-burning, but also being mixed with O-burning products. The regions with lower Si abundance are mainly the relatively faint parts of the remnant and might be dominated by the shocked circumstellar medium (CSM). We note here that the southeast ejecta, which are highly enriched in Fe and are believed to be synthesized in complete explosive Si-burning, are only a small fraction of the total remnant. They do not affect much the correlation discussed above.

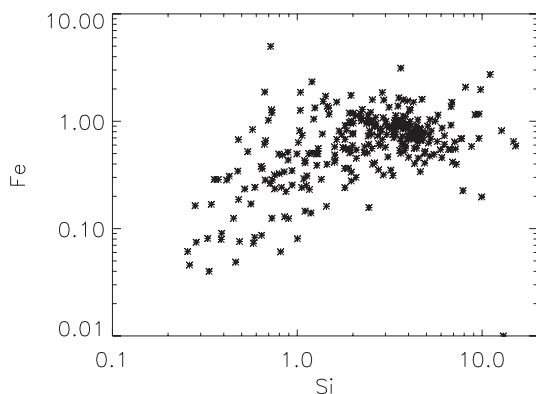


Fig. 10 Abundance correlation of Si versus Fe from regions with significant Fe-K lines.

5 SUMMARY

We carried out a spatially resolved X-ray spectroscopy of SNR Cas A. An obvious jet structure can be found in the Si, S and Ca abundance maps, which further confirms the previous suggestions. However, the Fe map shows that it does not follow the jet, but is distributed somehow perpendicular to it. Meanwhile, it lies outside the lighter elements (such as Si and S), which is consistent with the previous results and might be due to the neutrino-driven convection during the initiation of the SN explosion. The tight positive correlations among the Si, S and Ca abundances (Fig. 8) suggest that these elements come from explosive O-burning and incomplete Si-burning. The Ne and Mg abundances also show a good positive correlation, which means that they should be the ashes of explosive C/Ne burning. The Fe abundance is positively correlated with that of Si when the Si abundance is lower than 3 times the solar value, and is negatively correlated when the Si abundance is higher than 3. We propose that this two phase correlation is the result of the ways in which Fe is synthesized. The highly Si-enriched ejecta concentrated in the jet and the bright shell are probably a mixture of explosive O-burning and incomplete Si-burning products. The rest, in contrast, might be dominated by the shocked CSM.

Acknowledgements We acknowledge the data acquired by Chandra. The Chandra Observatory Center is operated by the Smithsonian Astrophysical Observatory for and on the behalf of NASA. This work is supported by the National Natural Science Foundation of China through Grants 10533020 and 10573017.

References

- Aschenbach B., 2002, In: Neutron Stars, Pulsars, and Supernova Remnants, ed. Becker W., Lesch H., and Trümper J. (MPE Rep. 278; Garching: MPE), 13
- Arnaud K. A., 1996, ASPC, 101, 17
- Anders E., Grevesse N., 1989, *Geochimica et Cosmochimica Acta*, 53, 197
- Bleeker J. A. M., Willingale R., van der Heyden K. J. et al., 2001, *A&A*, 365, L225
- Borkowski K. J., Lysterly W. J., Reynolds S. P., 2001, *ApJ*, 548, 820
- Fesen, R. A., Hurford A. P., 1996, *ApJS*, 106, 563
- Gotthelf E. V., Koralesky B., Rudnick L. et al., 2001, *ApJ*, 552, L39
- Hughes J. P., Rakowski C. E., Burrows D. N. et al., 2000, *ApJ*, 528, L109
- Hwang U., Holt S. S., Petre R., 2000, *ApJ*, 537, L119
- Hwang U., Laming J. M., 2003, *ApJ*, 597, 362
- Hwang U., Laming J. M., Badenes C. et al., 2004, *ApJ*, 615, L117
- Keohane J. W., Rudnick L., Anderson M. C., 1996, *ApJ*, 466, 309
- Klein R. I., Budil K. S., Perry T. S. et al., 2003, *ApJ*, 583, 245
- Klein R. I., McKee C. F., Colella P., 1994, *ApJ*, 420, 213
- Khokhlov A. M., Höflich P. A., Oran E. S. et al., 1999, *ApJ*, 524, L107
- Laming J. M., 2001, *ApJ*, 546, L1149
- Laming J. M., Hwang U., 2003, *ApJ*, 597, 347
- McKee C. F., 1974, *ApJ*, 188, 335
- Morrison R., McCammon D., 1983, *ApJ*, 270, 119
- Nagasaki S., Mizuta A., Yamada S. et al., 2003, *ApJ*, 596, 401
- Poludnenko A. Y., Frank A., Blackman E. G., 2002, *ApJ*, 576, 832
- Poludnenko A. Y., Dannenberg K. K., Drake R. P. et al., 2004, *ApJ*, 604, 213
- Reed J. E., Hester J. J., Fabian A. C. et al., 1995, *ApJ*, 440, 706
- Shklovsky I. S., 1973, *Soviet Astron.*, 16, 749
- Suh J. A., Audard M., Güdel M. et al., 2005, *ApJ*, 630, 1074
- Thielemann F.-K., Nomoto K., Hashimoto M., 1996, *ApJ*, 460, 408
- Thorstensen J. R., Fesen R. A., van den Bergh S., 2001, *AJ*, 122, 297
- Vink J., Kaastra J. S., Bleeker J. A. M., 1996, *A&A*, 307, L41
- Vink J., 2004, *New Astro. Rev.*, 48, 61
- Wang C. Y., Chevalier R. A., 2001, *ApJ*, 549, 1119
- Willingale R., Bleeker J. A. M., van der Heyden K. J. et al., 2002, *A&A*, 381, 1039
- Woolley S. E., Heger A., Weaver T. A., 2002, *Rev. Mod. Phys.*, 74, 1015
- Woolley S. E., Janka T., 2005, *Nat. Phys.*, 1, 147
- Woolley S. E., Weaver T. A., 1995, *ApJS*, 101, 181
- Zhang W., Woolley S. E., Heger A., 2004, *ApJ*, 608, 365